Title

Ultrafast Intersystem Crossing in Acetylacetone via Femtosecond X-ray Transient Absorption at the Carbon K-Edge

Journal

Journal of the American Chemical Society, 139(46)

ISSN

0002-7863

Authors

Bhattacherjee, Aditi
Pemmaraju, Chaitanya Das
Schnorr, Kirsten
et al.

Publication Date

2017-11-22

DOI

10.1021/jacs.7b07532

Peer reviewed

Ultrafast Intersystem Crossing in Acetylacetone via Femtosecond X-ray Transient Absorption at the Carbon K-edge

Aditi Bhattacherjee,[†,‡,|] Chaitanya Das Pemmaraju,[§] Kirsten Schnorr,[†,‡] Andrew R. Attar,[†,‡] and Stephen R. Leone*[†,‡,ǂ]

[†] *Department of Chemistry, University of California, Berkeley, California 94720, USA*

[‡] *Chemical Sciences Division, Lawrence Berkeley National Laboratory, Berkeley, California 94720, USA*

[§] *Theory Institute for Materials and Energy Spectroscopies, SLAC National Accelerator Laboratory, Menlo Park, California 94025, USA*

[ǂ] *Department of Physics, University of California, Berkeley, California 94720, USA*

Submitted to

Journal of the American Chemical Society

AUTHOR EMAIL ADDRESS: abhattacherjee@lbl.gov, dasc@slac.stanford.edu, kschnorr@berkeley.edu, andrewattar@berkeley.edu, srl@berkeley.edu

*A**ddress for correspondence:**

Prof. Stephen R. Leone

E-mail: srl@berkeley.edu

Telephone: (510)-643-5467, Fax: (510)-643-1376

[|] Present address: School of Chemistry, University of Bristol, Bristol BS8 1TH, United Kingdom.

Abstract:

Molecular triplet states constitute a crucial gateway in the photochemical reactions of organic molecules by serving as a reservoir for the excess electronic energy. Here, we report the remarkable sensitivity of soft x-ray transient absorption spectroscopy for following the intricate electronic structure changes accompanying the non-adiabatic transition of an excited molecule from the singlet to the triplet manifold. Core-level x-ray spectroscopy at the carbon-1s K-edge (284 eV) is applied to identify the role of the triplet state (T_1, $^3\pi\pi^*$) in the ultraviolet-induced photochemistry of pentane-2,4-dione (acetylacetone, AcAc). The excited-state dynamics initiated at 266 nm ($^1\pi\pi^*$, S_2) is investigated with element- and site-specificity using broadband soft x-ray pulses produced by high harmonic generation, in combination with time-dependent density functional theory calculations of the x-ray spectra for the excited electronic singlet and triplet states. The evolution of the core-to-valence resonances at the carbon K-edge establishes an ultrafast population of the T_1 state ($^3\pi\pi^*$) in AcAc via intersystem crossing on a 1.5 ± 0.2 ps timescale.

Introduction:

In a vast majority of organic chromophores, light-induced chemical reactions proceed from an intermediate electronic state that is different from the one that is directly excited. Rapid energy relaxation leads to the population of energetically low-lying electronic states, often with different spin multiplicities, which determine the final reaction outcome. For example, the photochemistry of unsaturated organic carbonyl compounds in the ultraviolet is complex with competing processes of internal conversion (IC) and intersystem crossing (ISC).[1] Besides providing an efficient pathway for energy relaxation, the rich and varied photochemistry in these molecules also encompasses rapid intramolecular rearrangement, Norrish-type cleavage and even elimination reactions.[2-3] Understanding the photochemistry of these molecules is important to elucidate key aspects of energy relaxation, photoisomerization, excited-state proton transfer, charge transfer, and coupled electronic-nuclear dynamics.

Scheme 1: Keto-enol tautomerism in Acetylacetone (AcAc). The enol form is stabilized in the gas phase by a strong intramolecular O-H···O hydrogen bond.

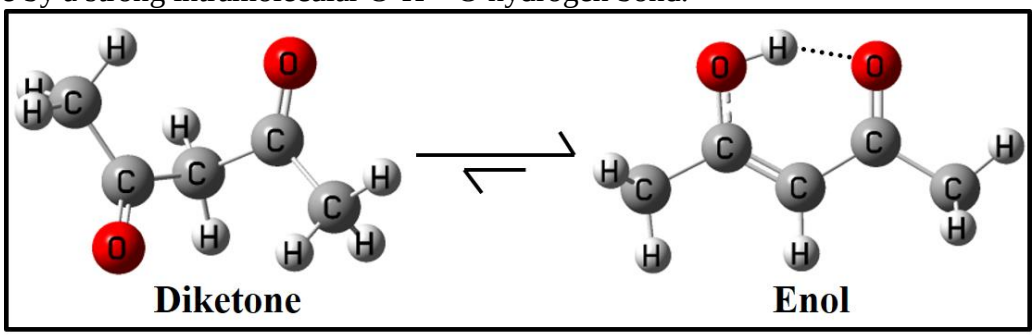

2,4-Pentanedione (or acetylacetone, abbreviated AcAc, Scheme 1) is a β-diketone that exhibits keto-enol tautomerism. The enolic (E) form of AcAc, the dominant tautomer in the gas phase (>93%),[4] is an α,β-enone that is stabilized by a strong (~12 kcal mol^{-1}) intramolecular hydrogen bond (Scheme 1).[5] The oscillator strength underlying the broad structureless absorption of AcAc in the ultraviolet that peaks at 263 nm is attributed to a $S_0 \rightarrow S_2(\pi\pi^*)$ transition in the

enolic form.[6] Following preparation of this bright state, the molecule undergoes rapid internal conversion to a lower-lying $^1n\pi^*$ (S_1) state.[7] The dominant reaction at this excitation wavelength is the unimolecular dissociation reaction to generate hydroxyl and 3-penten-2-on-4-yl radicals via a series of excited electronic states.[3, 8] Experimentally, the lowest triplet state has been invoked to explain the rotational energy distribution of the product OH radical in the photodissociation of AcAc, which is probed by laser-induced fluorescence.[8-9] The T_1 state is proposed to be a common intermediate in both the 266- and 248-nm photolysis of AcAc.[10] The theoretical reaction pathway proposed (depicted in Figure 1) for this reaction indeed reinforces the picture of non-adiabatic population transfer from the excited singlet to the triplet state following internal conversion, and calculations even reveal the possibility of a triple $S_1/T_1/T_2$ curve-crossing region.[11] However, the role of the triplet state in the ultraviolet-induced energy relaxation of AcAc lacks direct experimental evidence. Ultrafast electron diffraction studies suggest the involvement of a long-lived intermediate state (S_1, $n\pi^*$), which decays with a time-constant of 247 ± 34 ps to form the hydroxyl radical, presumably via slow intersystem crossing ($S_1 \rightarrow T_1$).[3] A femtosecond photoelectron spectroscopy study investigated the internal conversion dynamics upon photoexcitation at 266 nm and characterized the time-constants for the initial departure from the Franck-Condon region on the S_2 state (70 ± 10 fs) and the non-adiabatic population transfer from S_2 to S_1 (1.4 ± 0.2 ps).[7] A slow decay of the S_1 state was reported (up to 80 ps); however, the triplet state could not be observed due to a lack of an appropriate ionizing probe wavelength.

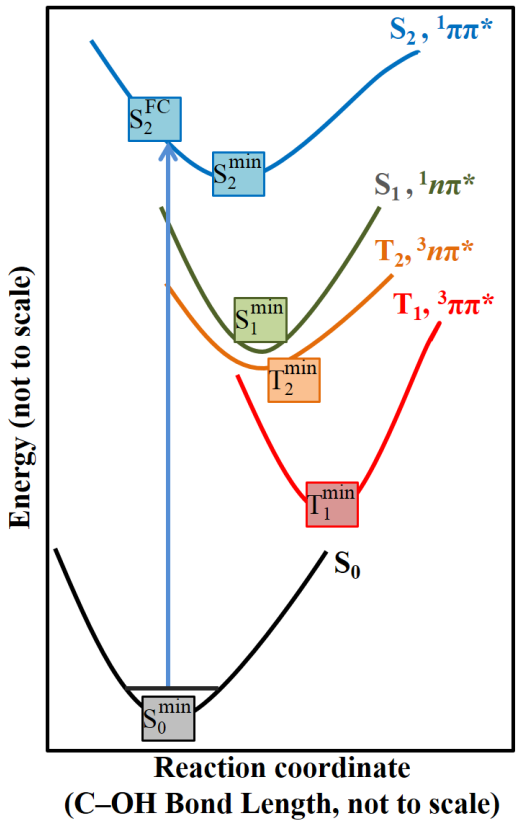

Figure 1: Schematic representation of the potential energy diagram of the ultraviolet-induced photochemistry of E-AcAc along the reaction co-ordinate (C-OH bond extension) for hydroxyl radical elimination (curve crossings are not shown). Multiple electronic states are involved and the electronic characters of the excited states are shown. Representative Franck-Condon (FC)-excited and stationary points (min) are indicated on the electronic state surfaces for which the x-ray spectra are simulated. T_1 and T_2 are found to be purely $\pi\pi^*$ and $n\pi^*$, respectively; however, S_1 and S_2 change character on the potential energy surface (see Figure S5 for details). The electronic energy provided by the pump pulse is redistributed over the vibrational modes of the molecule such as the OH stretch, C-O-H bend, C=C-O-H torsion modes[7] during excited-state relaxation (the one-dimensional schematic shown above does not reflect these normal modes).

Clearly, the inter-system crossing to the triplet-state manifold is a crucial element in the photochemistry of E-AcAc that remains to be investigated experimentally. Triplet state photochemistry is also common to a host of reaction systems such as fluorescence blinkers,[12] nucleobases,[13-14] and light-harvesting complexes.[15] Recent progress in the generation of soft x-ray pulses with table-top sources has opened up new avenues in soft x-ray absorption spectroscopy (XAS) at unprecedented timescales.[16-20] Time-resolved x-ray spectroscopy is a

powerful probe of electronic and structural dynamics in molecules and molecular complexes.[21-24] Electronic transitions from localized core-levels with well-defined orbital symmetries and angular momenta are inherently element-specific and also related to the charge distribution/spin of the initial and core-excited states through transition dipole matrix elements and exchange correlation.[25-26] Thus, when combined with time-resolved detection, the evolving near-edge core-to-valence spectral features report accurately on the changes in the electronic charge distributions, oxidation states, chemical environments, and spin crossover of the photoexcited molecule with atomic site specificity.[19, 27-41] Further, the large energy separations between the absorption edges of different elements (tens to hundreds of eV) and the encoding of the near-edge spectral region by a few predominant core-to-valence transitions offer easy spectral elucidation in comparison to valence state photoionization spectroscopies, which may produce broad and overlapping spectral signatures from multiple photoionization channels.[42] The high photon energies and bandwidth of the x-ray probe allows monitoring large amplitude nuclear motions on multiple electronic states, making core-level spectroscopy generally sensitive to geometrical parameters and charge states.[27, 43-45] Here, we use femtosecond soft x-ray transient absorption spectroscopy to probe the ultrafast non-adiabatic population transfer into the triplet state after initial excitation of E-AcAc to the optically bright $^1\pi\pi^*$ (S_2) state. The sensitivity of the core-to-valence pre-edge resonances to the nature of the valence-excited states in polyatomic molecules provides valuable electronic structure insights into the photochemical reaction pathways and transition states.[42, 46-47] We report the photoexcited dynamics of AcAc by following the evolution of the key core-to-valence resonance peaks in the x-ray absorption spectra at the carbon K-edge and comparing them with TDDFT-simulated x-ray spectra of the

excited states. The results show that the non-adiabatic passage to the T_1 state in AcAc is ultrafast and occurs much more rapidly than previously thought.

Methods:

A detailed description of the experimental and computational methodologies is included in the Supporting Information (Figure S1-S4). Briefly, 266 nm pulses (5-7 μJ per pulse, corresponding to pump intensities of 1.2×10^{11} to 1.7×10^{11} Wcm^{-2}) are used to excite the gas-phase AcAc molecules, which are then probed using temporally-delayed, broadband, soft x-ray pulses at the carbon K-edge (high harmonics of a 1320 nm optical parametric amplifier output pumped by a Ti:sapphire laser). The differential soft x-ray absorption spectra are acquired in shorter time intervals up to 10 ps, and at longer intervals between 10 to 150 ps. An *in-situ* cross-correlation of the pump and probe pulses is determined by the ponderomotive shift of the core-excited Rydberg states of Argon, which yields the time-zero and the instrument response function (IRF, 90 fs) of the apparatus.

Near-edge x-ray absorption fine structure (NEXAFS) spectra are calculated for fixed molecular geometries corresponding to the ground-state minimum, FC-excited and stationary points on the excited electronic state surfaces using a previously demonstrated methodology[19] that combines the restricted energy-window[48] linear-response time-dependent density functional theory (TDDFT) formalism[49] for core-excited states with the maximum overlap method (MOM)[50-51] for valence-excited states. The restricted energy-window TDDFT formalism has been widely applied over the past few years to study near-edge x-ray excitation spectra in molecules,[48, 52] including recent applications to corroborate transient x-ray absorption experiments.[19, 53] Simulations are carried out at the CAM-B3LYP/aug-cc-pvdz level for molecular geometries reported by Chen et al. using a Complete Active Space Self-Consistent

Field (CASSCF) calculation.[11] Calculations of the NEXAFS spectra do not account for any possible vibrational excitation; however, these single-point calculations serve as a reasonable starting point. The computed ground-state NEXAFS is uniformly offset by 10.3 eV to higher energies in order to align with the experimental NEXAFS spectrum. A constant blue-shift of 10.3 eV is also applied to the computed spectra for all excited electronic states. In DFT functionals of the type we employ, the absolute binding energy of the C 1s core-state is underestimated (errors in the range of ~10 eV). The rigid energy shift therefore acts as a calibration parameter that simply corrects for (without affecting the relative positions of any peaks) a known systematic error in the energy of the C 1s core-states that are common to all x-ray transitions. The use of approximate exchange-correlation functionals and spin-contamination effects inherent to a single-determinant TDDFT treatment of excited states are expected to lead to uncertainties in the range of ~0.3 eV for the predicted transition energies.

Results and Discussion:

Figure 2 shows a comparison of the NEXAFS spectrum of AcAc (S_0) at the carbon K-edge with the TDDFT-calculated result for the enol tautomer. The stick spectrum displays the prominent calculated core-valence transitions of the constituent carbon atoms (C_3 in red, C_2 in blue, C_4 in green, and terminal methyl carbons in yellow) underlying the peaks in the observed NEXAFS spectrum (solid black line). The individual sticks are broadened with a Gaussian width of 0.2 eV to obtain the shaded-gray spectrum. The lowest energy peak in the experimental NEXAFS, observed at 284.4 eV, is assigned to a 1s(C_3)→π*(LUMO) transition. The second peak, identified at 286.6 eV, is assigned to two energetically close-lying 1s(C_2)→π*(LUMO) and 1s(C_4)→π*(LUMO) transitions. The greater core-LUMO resonance energies for the $C_{2,4}$ atoms in comparison to C_3 are due to a chemical shift of the binding energy of the core-1s electrons

from the proximity of the $C_{2,4}$ atoms to the more electronegative (oxygen) heteroatoms.[54-55] A third peak at 288.2 eV is discernible along the rising carbon K-edge, which corresponds to overlapping transitions of the 1s core-electrons of C_1, C_3, and C_5 to higher unoccupied valence orbitals (All computed peaks over 287 eV arise from transitions to higher unoccupied valence and Rydberg-type orbitals). The TDDFT-computed spectrum of the enol tautomer reproduces all three peaks in the experimental NEXAFS with remarkably good relative accuracy (within 0 to 0.1 eV). The high energy peaks greater than 289 eV in the computed spectrum are not observed in the experiment due to the rising edge that results from ionization of the core-1s electrons. For comparison, the computed NEXAFS spectrum of the diketo tautomer is provided in Figure S6 where the first core-valence resonance is expected to occur only at 286.5 eV, corresponding to a $1s(C_{2,4})\rightarrow\pi^*$(LUMO) transition. Thus, the peak observed at 284.4 eV in the experimental NEXAFS spectrum confirms the existence of the enol tautomer in the gas phase. Because of the close similarity in the calculated energies and oscillator strengths of the core-valence transitions in the enol and dione tautomers at energies greater than 286 eV, it is not possible to extract a meaningful keto-enol ratio from the experimental NEXAFS spectrum. However, as the enolic tautomer is known to solely contribute to the 266 nm absorption peak in the UV (the diketone absorption lies above 290 nm),[6] all changes in absorbance observed in the pump-probe spectra, *vide infra*, are solely attributed to the enol tautomer. Therefore, the use of AcAc in the rest of the paper refers specifically to the enol tautomer.

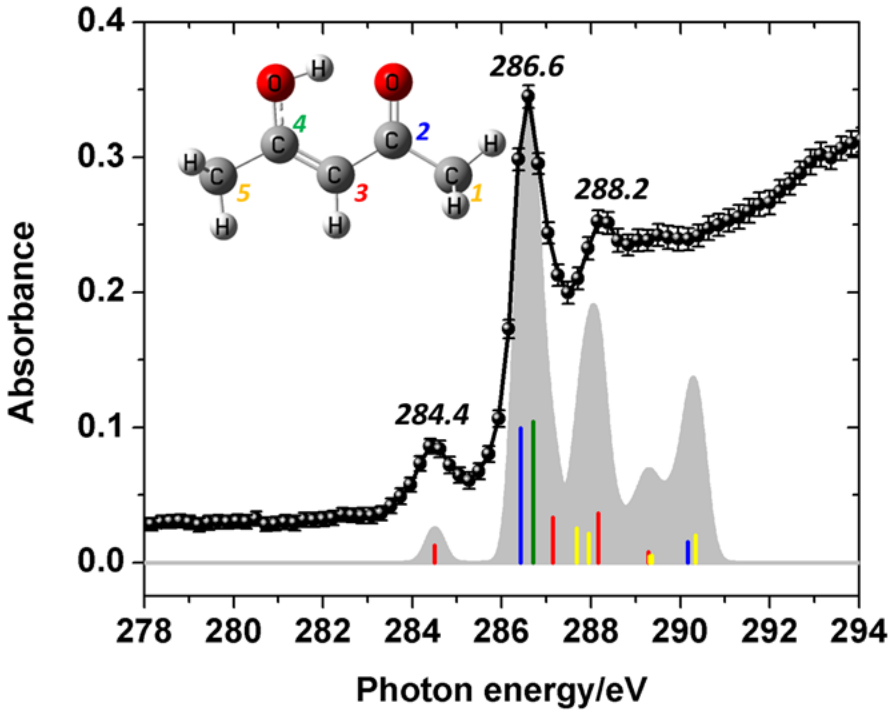

Figure 2: Static near-edge x-ray absorption fine structure (NEXAFS) spectrum of AcAc in the S_0 state (solid black line connecting the data points, error bars correspond to 95% confidence interval over 64 spectra). The calculated (TDDFT) stick spectrum of the enolic tautomer (uniformly shifted to higher energies by 10.3 eV to match the experimental spectrum) shows the specific carbon atoms participating in the prominent core-valence transitions (inset shows the atom numbering scheme; see text for assignment). A Gaussian broadening of 0.2 eV is applied to the stick spectrum to obtain the shaded-gray spectrum. The intensity scale of the computed spectrum is normalized to the strongest peak (286.6 eV) in the experimental NEXAFS. An energy cut-off is imposed in the calculations at 291 eV.

Figure 3(a) shows a two-dimensional contour map of the transient x-ray absorption spectrum of AcAc upon 266 nm excitation for time delays between -500 fs and 10 ps, where yellow-red and blue-black contours denote positive and negative ΔA features, respectively. The averaged differential-absorption spectra over three representative time-windows (120-200 fs in blue, 1.2-2 ps in green, and 7-10 ps in red; Figure 3b), each referenced against the ΔA spectrum at negative time-delays (-450 to -50 fs; gray line), further reveal the prominent features of the time-dependent x-ray spectra (the complete binning of the differential absorption spectra over distinct time-windows is provided in Figure S7). Six distinct features, numbered 1-6, are

identified in the near-edge over a 10-ps timescale. Up to ~1 ps following photoexcitation, depletion of the ground-state manifests at 286.6 eV (peak 5), and the concomitant rises of two peaks at 284.7 eV (peak 3) and 285.9 eV (peak 4) are observed. Depletion of the 1s(C_3)π* ground-state resonance at 284.4 eV (see static-NEXAFS, Figure 2) is not observed because of the overlapping positive ΔA peak at 284.7 eV. A weak and broad absorption peak also appears at 288.4 eV (peak 6). All four features (peaks 3-6) start to decay after about one picosecond as two new peaks begin to emerge at 281.4 eV (peak 1) and 283.8 eV (peak 2). The decay of peak 3 and the concomitant appearance of peak 2 manifests as a gradual red-shift in the contour map in the 1-2 ps region. This is also evident from the appearance of a low-energy wing of the 284.7 eV peak in the differential absorption spectrum in the 1.2-2 ps-timescale that transitions into the 283.8 eV peak at long time-delays (7-10 ps).

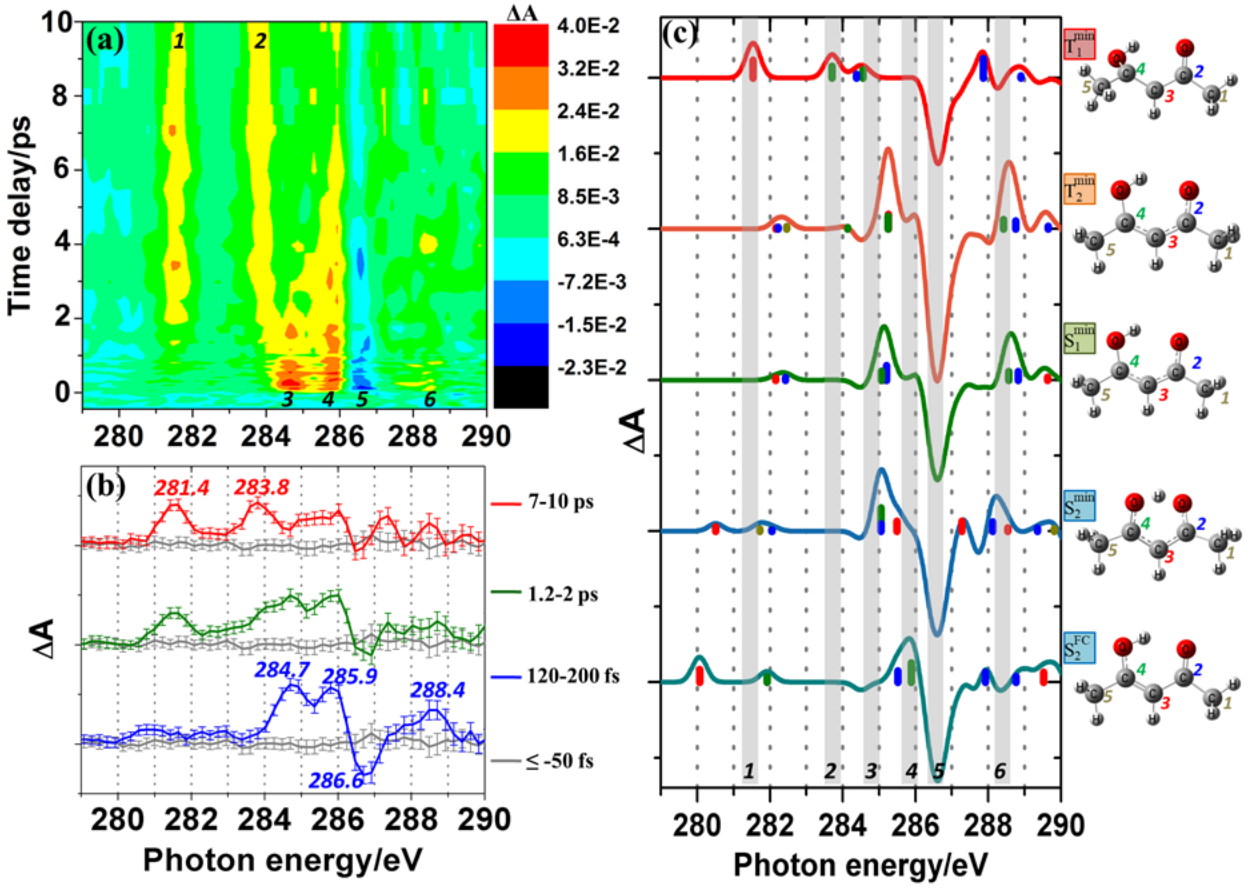

211

Figure 3:(a) Two-dimensional contour map of the experimentally measured 266 nm-induced excited-state dynamics in E-AcAc shows six notable features (labeled 1-6). The color key on the right provides the scale for the measured differential soft x-ray absorption (ΔA).**(b)** Experimental soft x-ray differential absorption spectra measured at different time-delays between the photoexcitation (266 nm pump) and soft x-ray (probe) pulses. Each spectrum represents the average differential absorption over the respective time-window and is referenced to the differential absorption measured at negative time-delays (gray line). Each division on the y-axis corresponds to 50 mΔA. Features over and below the gray line denote positive and negative ΔA features, respectively. The major peaks observed and discussed in the text are annotated. Error bars denote a 95% confidence limit of 24 spectra. **(c)** Computed (TDDFT) soft x-ray differential absorption spectra corresponding to the Franck-Condon (FC, S_2) and stationary state (min) structures of the excited-singlet and triplet states (each division on the y-axis corresponds to 50 mΔA). The spectra are obtained by subtracting the computed ground-state NEXAFS spectrum from the computed excited-state NEXAFS spectra and scaling down the intensity scale uniformly by 10% (accounting for uncertainties in the percentage of excited molecules at our sample densities, pump fluence, and focusing conditions) to match the ΔA scale of the experimental differential absorption spectra. The structures and atom-numbering are shown on the right.

To elucidate the multiple absorption features that appear in the transient absorption spectra at the carbon K-edge upon UV excitation of AcAc, the TDDFT-simulated differential-absorption spectra for representative geometries corresponding to the excited singlet (S_2 and S_1) and triplet (T_2 and T_1) states of AcAc are shown in Figure 3c (see Figure S8 for the computed NEXAFS spectra of the excited electronic states). The underlying stick spectra reveal the particular carbon atoms involved in the core-valence transitions, as per the color scheme introduced earlier (Figure 2), and a Gaussian broadening of 0.2 eV is applied. The positions of peaks 1-6 observed in the experiment are also highlighted in Figure 3(c) by vertical gray bars to guide the spectral assignment. Comparison of the observed transient absorption spectra (Figure 3b) with the TDDFT-simulated spectra (Figure 3c) reveals that the peak at 285.9 eV (peak 4) in the experimental differential-absorption spectrum likely originates from the FC region on the S_2 surface. In this region, the electrons are excited into a ππ* state, however, the nuclear geometry has not yet begun to respond to the electronic excitation. Photoexcitation into the ^{1}ππ* excited-state opens up a new lower-energy, half-filled π orbital for transition from the carbon 1s core-

electrons, which gives rise to the peaks at 280.1 eV and 281.9 eV in the computed spectrum (note that these peaks appear to the lower-energy side of the computed carbon K-edge absorption peaks in the S_0 state by approximately the UV excitation energy). Some weak absorption features between 280 and 283 eV can be noted in the experimental spectrum (120-200 fs), which appear smeared-out because of the finite experimental IRF (as the molecule exits the FC-region, the orbital character evolves from $\pi\pi^*$ to $n\pi^*$ which also leads to the broadening of these peaks, see Figure S5). Calculations reveal the peak at 285.9 eV in the FC-region corresponds to transitions of the 1s core-electrons of the C_2/C_4 atoms into unoccupied orbitals with mixed π- and Rydberg character. Following the gradient of the potential energy surface along the C(4)-O bond extension co-ordinate, the excited molecule departs from the FC region and approaches the energy-minimum of the S_2 state along the reaction co-ordinate. For this particular structure, two new peaks are predicted to occur at 285.1 eV and 288.2 eV. The former peak corresponds to overlapping transitions from the 1s-cores of C_4 and C_3 to unoccupied orbitals with mixed non-bonding and Rydberg character. The latter peak projects the 1s electrons of these carbon atoms onto higher unoccupied valence orbitals with partial Rydberg character. Meanwhile, the transitions of the core electrons into the frontier valence orbitals, π and π*, predicted to occur at 280.5 and 281.8 eV contribute to the weak and broad ΔA peaks between 280 and 283 eV.

The simulations further reveal that the internal conversion of the excited molecule to the S_1 state is only characterized by minor spectral changes in the region between 284 and 289 eV. For example, in the simulated x-ray spectra of the S_1 state, the peak at 285.1 eV (which projects the 1s electrons from the C_2, C_3, and C_4 atoms to unoccupied orbitals with mixed non-bonding and Rydberg character) remains, and a small blue-shift of the higher energy core-valence resonance peak to 288.6 eV is noted. Because of the significant spectral overlap of the predicted

core-valence resonances of the S_2 and S_1 states between 285 and 289 eV, peaks 3 and 6 are jointly assigned to the S_2 and S_1 states. The slight discrepancy (~0.4 eV) of peak 3 with the theoretical position is on the order of the spectrometer resolution (~0.3 eV). Due to the IRF (90 fs) of the apparatus and the overlapping nature of the computed x-ray peaks for the S_2-FC and relaxed $S_{2,1}$ geometries between 285 eV and 286 eV, the twin peaks observed in the experiment at 284.7eV (peak 3) and 285.9 eV (peak 4) are observed to rise and decay together. A shorter 266 nm pulse duration might make it possible to observe differences in the rise-times of these peaks. It is worth pointing out that the S_2/S_1 states possess $\pi\pi^*/n\pi^*$ character, respectively; hence following the temporal evolution of the delocalized $1s\rightarrow\pi$ and localized $1s\rightarrow n$ core-valence transition at the oxygen K-edge (543 eV) in the future will allow confirming the internal conversion dynamics in AcAc, which has been well studied.[7] There is also significant spectral overlap of the computed core-valence resonances of the S_1 and S_2 states in the region between 284 and 289 eV with the theoretical x-ray spectra of the T_2 state and the product radical (Figure S9-S10), however, these are expected to rise in later and be much longer-lived than the singlet states. Hence their contribution to the peak amplitudes of peaks 3, 4 and 6 are expected to be negligible immediately after photoexcitation, although there might be some finite contribution at longer time-delays (perhaps explaining the residual differential absorption at these energies in the 7-10-ps window).

The ΔA spectra measured in the long-delay limit (7-10 ps, Figure 3b) show characteristic new resonances at 281.4 eV (peak 1) and 283.8 eV (peak 2), which are not present at early times (< 500 fs). The differential absorption spectrum in the 1.2-2 ps time-window marks their onset. These spectroscopic features are in good agreement with the TDDFT-calculated core-valence transition energies of the T_1 state energy-minimum (Figure 3c). The calculated spectrum

indicates that the x-ray absorption peaks in the T_1 state arise from electronic excitation of the core-1s electrons of C_3 into the unoccupied valence (π) and the core electrons from $C_{2,4}$ into mixed π- and Rydberg-type orbitals. Chen et al. report that rotational isomerization can easily proceed on the T_1 surface (presumably due to single-bond character of the C_3-C_4 bond), giving rise to five different conformers (CCT, CTC, CTT, TCC, and TCT).[11] Calculation of the x-ray spectra of these rotational isomers indicates the coalescence of the second (283.7 eV) and third peaks (284.5 eV) of the T_1 spectrum into a single peak (284.1 eV, Figure S10), with a minor increase in oscillator strength. However, due to the large vibrational broadening of the experimentally observed x-ray absorption peaks (full-width-at-half-maximum of 0.9 eV for the 283.7 eV feature), the presence of the rotational isomers in the experiment cannot be directly observed. Nonetheless, the agreement between the observed spectral positions of peaks 1 and 2 with those of the T_1 state leads to unambiguous identification of non-adiabatic population transfer into T_1. The sensitivity of peaks 1 and 2 to geometrical and electronic changes is independently verified by sampling different geometries on the T_1 state (Figure S11) and for a different electronic structure at the T_1^{min} geometry (Figure S12). Both the peak positions and peak amplitudes are seen to significantly differ with variations in geometrical (up to ~1 eV) and electronic changes (up to ~500 meV), which reflects the general sensitivity of x-ray spectroscopy to geometrical parameters and orbital character. It must be noted that intersystem crossing from the S_1 ($^1n\pi^*$) state to the T_1 ($^3\pi\pi^*$) state is allowed according to El-Sayed's rules[56] since the spin-flip is accompanied by a change in orbital angular momentum; however, it is forbidden to the T_2 ($^3n\pi^*$) state, as also noted for many other organic molecules.[1, 56-58] A new peak at 287.4 eV, although barely evident in Figure 3b, gains prominence at longer timescales (10-100 ps, Figure S13) and is possibly also arising from the T_1 state; the computed spectrum of this state predicts

an absorption peak at 287.8 eV (within experimental resolution). In fact, it appears that the seeming recovery of the ground-state bleach (peak 5) also owes its origin to an overlapping resonance with the T_1 state (which gives rise to peaks 1 and 2), as all three peaks are characterized by similar temporal behavior. Although an $S_2 \rightarrow T_2 \rightarrow T_1$ reaction pathway is also allowed by El-Sayed's rules, an initial IC followed by ISC is expected to be kinetically favored because of the lower S_2/S_1 energy gap and a likely S_2/S_1 conical intersection (as seen in the case of malonaldehyde).[3, 11, 59-60] Previous ultrafast experiments[3, 7] and theoretical studies[11] point towards IC as the predominant S_2 relaxation pathway in AcAc. A sequential photophysical process characterized by an ultrafast $S_2 \rightarrow S_1$ relaxation followed by ISC is also noted for several α,β-enones.[1, 61]

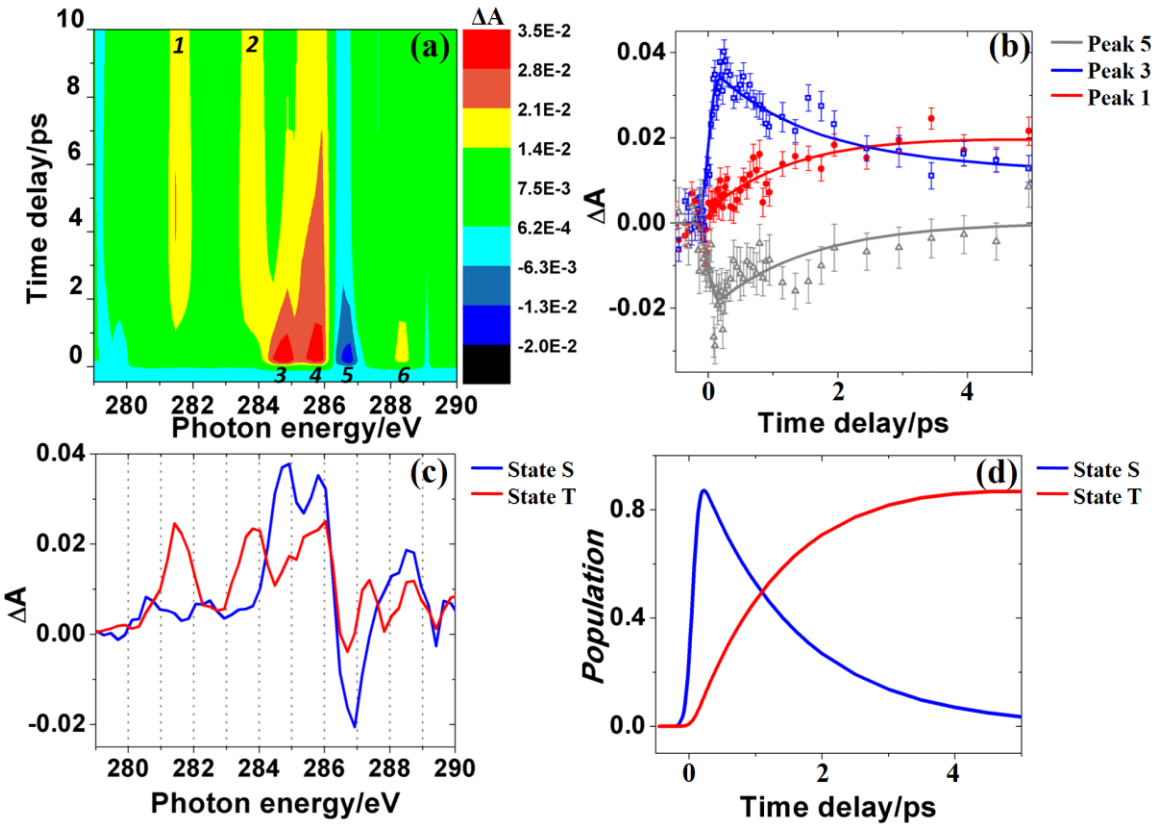

Figure 4:(a) Reconstructed 2D-contour map from a global fit of the transient absorption spectrum using a sequential two-state (S→T) model. **(b)** Global fits (solid lines) to the time-dependent amplitudes of representative peaks 1, 3, and 5 in the transient x-ray absorption spectra

(error bars correspond to 95% confidence interval of 24 measured ΔA spectra) **(c)** Evolution associated spectra for the two states S and T in the model **(d)** Population evolution of states S and T.

A global fitting tool[62] based on a singular-value decomposition method reveals the kinetics of the ultrafast non-adiabatic population transfer into the T_1 state of AcAc (Figure 4). A sequential two-state model ($S_{2/1} \rightarrow T_1$) with a 90 fs IRF is applied. It yields an excellent match with the observed transient absorption spectra as seen from the reconstructed contour plot up to 10 ps (Figure 4a) where all of the major peaks 1-6 can be identified. Representative kinetics traces of key resonance features observed at 281.4 eV (peak 1), 284.7 eV (peak 3), and 286.6 eV (peak 5) are shown in Figure 4(b) (see Figure S14 for kinetics traces of the other peaks). The evolution associated spectra for the two states in the model (combined S_2/S_1 and T_1) and the time-dependent populations are shown in Figures 4c and 4d, respectively (fits to the experimental differential absorption spectra at different time-delays are shown in Figure S15). The global fit identifies an ISC rate ($1/k$) of 1.5 ± 0.2 ps (one standard error calculated by the root-mean-square method), revealing fast intersystem crossing in AcAc. Other relevant studies of linear and cyclic enones indicate ISC rates ranging from ~1 to 3 ps, consistent with the results here.[1, 63] Since the stationary point structures of the S_1 and S_2 states are seen to have close-lying core-valence resonances between 285 and 289 eV, the individual $S_2 \rightarrow S_1$ IC step in the reaction pathway cannot be directly determined in the transient x-ray absorption data. Complementary x-ray absorption with compressed 266 nm pulses and/or x-ray photoemission/Auger spectroscopy experiments can be combined in the future to follow population transfer over multiple excited states.[64] Also, high harmonic probe energies spanning the 'water-window' region can provide a complementary picture of the photochemical reaction by monitoring the core-valence resonances at the oxygen K-edge (543 eV), especially for electronic states with $n\pi^*$ character since the non-bonding orbital is localized on the O atom.[65]

Conclusion:

Time-resolved x-ray absorption spectroscopy using a broadband carbon K-edge high-harmonic probe reveals an ultrafast intersystem crossing in the 266 nm-photoexcitation of AcAc that populates the triplet (T_1) state on a sub-2 ps time-scale. The nature of coupling between the $S_2/S_1/T_1$ states (vibronic or conical intersection) remains to be identified by high-level ab initio theory. Nonetheless, the ability of core-level spectroscopy to investigate the non-adiabatic dynamics in polyatomic molecules with multiple excited states is clearly revealed. This detection method is largely universal, being independent of frequently encountered experimental difficulties in pump-probe techniques such as the unfavorable ionization cross-sections of the triplets[66] or the presence of high-lying Rydberg states used to mediate the ionization pathway.[67] The method is able to directly distinguish between multiple electronic states by projecting localized core-electrons onto unoccupied valence orbitals in an element- and site-specific manner via chemical shifts. The detection of different spin states should be tractable by x-ray spectroscopy for other chromophores as well, as long as the energy separation between the states is greater than the experimental spectral resolution. Even for near-degenerate electronic states, which are characterized by different electronic structures (example, $\pi\pi$ and $n\pi^*$), complementary carbon and oxygen (or heteroatom) K-edge spectra can provide unique element- and orbital-specific spectral signatures to unambiguously identify the electronic states, and track the associated population/relaxation timescales. These results shed light on the applicability of time-resolved x-ray absorption spectroscopy as a powerful probe to elucidate complex non-adiabatic dynamics in photoexcited polyatomic molecules and pave the way for a universal detection scheme of reactive triplets and other metastable electronic states.

Supporting Information:

Experimental and computational methods; detailed NEXAFS and x-ray transient absorption spectra; kinetic and spectral fits to the experimental data from global fitting.

Acknowledgement:

This research work, A.B. and A.R.A. were supported by the U.S. Department of Energy, Office of Science, Office of Basic Energy Sciences (Contract No. DE-AC02-05CH11231), the gas phase chemical physics program through the Chemical Sciences Division of Lawrence Berkeley National Laboratory. The apparatus was partially funded by a NSF ERC, EUV Science and Technology, under a previously completed grant (No. EEC-0310717). C.D.P. performed the computational work within TIMES at SLAC, supported by the U.S. Department of Energy, Office of Basic Energy Sciences, Division of Materials Sciences and Engineering, under Contract No. DE-AC02-76SF00515. Computational simulations were carried out on the Sherlock cluster administered by the Stanford Research Computing Center. K.S. was supported by a Peter Paul Ewald Fellowship from the Volkswagen Foundation.

References:

1. Schalk, O.; Schuurman, M. S.; Wu, G.; Lang, P.; Mucke, M.; Feifel, R.; Stolow, A., *J. Phys. Chem. A* **2014**, *118*, 2279-2287.

2. Wu, W.; Yang, C.; Zhao, H.; Liu, K.; Su, H., *J.Chem. Phys.* **2010**, *132*, 124510.

3. Xu, S. J.; Park, S. T.; Feenstra, J. S.; Srinivasan, R.; Zewail, A. H., *J. Phys. Chem. A* **2004**, *108*, 6650-6655.

4. Irving, R. J.; Wadso, I., *Acta Chem. Scand.* **1970**, *24*, 589-592.

5. Dannenberg, J. J.; Rios, R., *J. Phys. Chem.* **1994**, *98*, 6714-6718.

6. Nakanishi, H.; Morita, H.; Nagakura, S., *Bull. Chem. Soc. Jpn.* **1977**, *50*, 2255-2261.

7. Poisson, L.; Roubin, P.; Coussan, S.; Soep, B.; Mestdagh, J. M., *J. Am. Chem. Soc.* **2008**, *130*, 2974-2983.

8. Yoon, M. C.; Choi, Y. S.; Kim, S. K., *Chem. Phys. Lett.* **1999**, *300*, 207-212.

9. Yoon, M. C.; Choi, Y. S.; Kim, S. K., *J.Chem. Phys.* **1999**, *110*, 11850-11855.

10. Upadhyaya, H. P.; Kumar, A.; Naik, P. D., *J.Chem. Phys.* **2003**, *118*, 2590-2598.

11. Chen, X. B.; Fang, W. H.; Phillips, D. L., *J. Phys. Chem. A* **2006**, *110*, 4434-4441.

12. Basche, T.; Kummer, S.; Brauchle, C., *Nature* **1995**, *373*, 132-134.

13. Barbatti, M.; Aquino, A. J. A.; Szymczak, J. J.; Nachtigallova, D.; Hobza, P.; Lischka, H., *Proc. Natl. Acad. Sci. USA* **2010**, *107*, 21453-21458.

14. Mai, S.; Pollum, M.; Martinez-Fernandez, L.; Dunn, N.; Marquetand, P.; Corral, I.; Crespo-Hernandez, C. E.; Gonzalez, L., *Nat. Commun.* **2016**, *7*, 13077.

15. Gradinaru, C. C.; Kennis, J. T. M.; Papagiannakis, E.; van Stokkum, I. H. M.; Cogdell, R. J.; Fleming, G. R.; Niederman, R. A.; van Grondelle, R., *Proc. Natl. Acad. Sci. USA* **2001**, *98*, 2364-2369.

16. Cousin, S. L.; Silva, F.; Teichmann, S.; Hemmer, M.; Buades, B.; Biegert, J., *Opt. Lett.* **2014**, *39*, 5383-5386.

17. Silva, F.; Teichmann, S. M.; Cousin, S. L.; Hemmer, M.; Biegert, J., *Nat. Commun.* **2015**, *6*, 6611.

18. Teichmann, S. M.; Silva, F.; Cousin, S. L.; Hemmer, M.; Biegert, J., *Nat. Commun.* **2016**, *7*, 11493.

19. Attar, A. R.; Bhattacherjee, A.; Pemmaraju, C. D.; Schnorr, K.; Closser, K. D.; Prendergast, D.; Leone, S. R., *Science* **2017**, *356*, 54-59.

20. Pertot, Y.; Schmidt, C.; Matthews, M.; Chauvet, A.; Huppert, M.; Svoboda, V.; von Conta, A.; Tehlar, A.; Baykusheva, D.; Wolf, J. P.; Wörner, H. J., *Science* **2017**, *355*, 264-267.

21. Bressler, C.; Chergui, M., *Chem. Rev.* **2004**, *104*, 1781-1812.

22. Bressler, C.; Chergui, M., *Ann. Rev. Phys. Chem.* **2010**, *61*, 263–268.

23. Milne, C. J.; Penfold, T. J.; Chergui, M., *Coord. Chem. Rev.* **2014**, *277*, 44–68.

24. Chen, L. X.; Zhang, X.; Shelby, M. L., *Chem. Sci.* **2014**, *5*, 4136-4152.

25. Stöhr, J., *NEXAFS Spectroscopy* **1996**, *Springer Series in Surface Sciences*.

26. Baker, M. L.; Mara, M. W.; Yan, J. J.; Hodgson, K. O.; Hedman, B.; Solomon, E. I., *Coord. Chem. Rev.* **2017**, *345*, 182-208.

27. Gawelda, W.; Johnson, M.; de Groot, F. M. F.; Abela, R.; Bressler, C.; Chergui, M., *J. Am. Chem. Soc.* **2006**, *128*, 5001-5009.

28. Gawelda, W.; Pham, V. T.; Benfatto, M.; Zaushitsyn, Y.; Kaiser, M.; Grolimund, D.; Johnson, S. L.; Abela, R.; Hauser, A.; Bressler, C.; Chergui, M., *Phys. Rev. Lett.* **2007**, *98*, 057401.

29. Ochmann, M.; von Ahnen, I.; Cordones, A. A.; Hussain, A.; Lee, J. H.; Hong, K.; Adamczyk, K.; Vendrell, O.; Kim, T. K.; Schoenlein, R. W.; Huse, N., *J. Am. Chem. Soc.* **2017**, *139*, 4797–4804.

30. Bressler, C.; Milne, C.; Pham, V.-T.; ElNahhas, A.; van der Veen, R. M.; Gawelda, W.; Johnson, S.; Beaud, P.; Grolimund, D.; Kaiser, M.; Borca, C. N.; Ingold, G.; Abela, R.; Chergui, M., *Science* **2009**, *323*, 489-492.

31. Huse, N.; Cho, H.; Hong, K.; Jamula, L.; de Groot, F. M. F.; Kim, T. K.; McCusker, J. K.; Schoenlein, R. W., *J. Phys. Chem. Lett.* **2011**, *2*, 880–884.

32. Van Kuiken, B. E.; Huse, N.; Cho, H.; Strader, M. L.; Lynch, M. S.; Schoenlein, R. W.; Khalil, M., *J. Phys. Chem. Lett.* **2012**, *3*, 1695-1700.

33. Katz, J. E.; Zhang, X.; Attenkofer, K.; Chapman, K. W.; Frandsen, C.; Zarzycki, P.; Rosso, K. M.; Falcone, R. W.; Waychunas, G. A.; Gilbert, B., *Science* **2012**, *337*, 1200-1203.

34. Vura-Weis, J.; Jiang, C. M.; Liu, C.; Gao, H.; Lucas, J. M.; de Groot, F. M. F.; Yang, P.; Alivisatos, A. P.; Leone, S. R., *J. Phys. Chem. Lett.* **2013**, *4*, 3667−3671.

35. Reinhard, M.; Penfold, T. J.; Lima, F. A.; Rittmann, J.; Rittmann-Frank, M. H.; Abela, R.; Tavernelli, I.; Rothlisberger, U.; Milne, C. J.; Chergui, M., *Struct. Dyn.* **2014**, *1*, 024901.

36. Zhang, W.; Alonso-Mori, R.; Bergmann, U.; Bressler, C.; Chollet, M.; Galler, A.; Gawelda, W.; Hadt, R. G.; Hartsock, R. W.; Kroll, T.; Kjær, K. S.; Kubicek, K.; Lemke, H. T.; Liang, H. W.; Meyer, D. A.; Nielsen, M. M.; Purser, C.; Robinson, J. S.; Solomon, E. I.; Sun, Z.; Sokaras, D.; van Driel, T. B.; Vanko, G.; Weng, T.-S.; Zhu, D.; Gaffney, K. J., *Nature* **2014**, *509*, 345-348.

37. Wernet, P.; Kunnus, K.; Josefsson, I.; Rajkovic, I.; Quevedo, W.; Beye, M.; Schreck, S.; Grubel, S.; Scholz, M.; Nordlund, D.; Zhang, W.; Hartsock, R. W.; Schlotter, W. F.; Turner, J.

J.; Kennedy, B.; Hennies, F.; de Groot, F. M. F.; Gaffney, K. J.; Techert, S.; Odelius, M.; Fohlisch, A., *Nature* **2015**, *520*, 78-81.

38. Van Kuiken, B. E.; Cho, H.; Hong, K.; Khalil, M.; Schoenlein, R. W.; Kim, T. K.; Huse, N., *J. Phys. Chem. Lett.* **2016**, *7*, 465−470.

39. Shelby, M. L.; Lestrange, P. J.; Jackson, N. E.; Haldrup, K.; Mara, M. W.; Stickrath, A. B.; Zhu, D.; Lemke, H. T.; Chollet, M.; Hoffman, B. M.; Li, X.; Chen, L. X., *J. Am. Chem. Soc.* **2016**, *138*, 8752−8764.

40. Mara, M. W.; Hadt, R. G.; Reinhard, M. E.; Kroll, T.; Lim, H.; Hartsock, R. W.; Alonso-Mori, R.; Chollet, M.; Glownia, J. M.; Nelson, S.; Sokaras, D.; Kunnus, K.; Hodgson, K. O.; Hedman, B.; Bergmann, U.; Gaffney, K. J.; Solomon, E. I., *Science* **2017**, *356*, 1276–1280.

41. Van Kuiken, B. E.; Ross, M. R.; Strader, M. L.; Cordones, A. A.; Cho, H. N.; Lee, J. H.; Schoenlein, R. W.; Khalil, M., *Struct. Dyn.* **2017**, *4*, 044021.

42. Neville, S. P.; Averbukh, V.; Patchkovskii, S.; Ruberti, M.; Yun, R.; Chergui, M.; Stolow, A.; Schuurman, M. S., *Faraday Discuss.* **2016**, *194*, 117-145.

43. Hosler, E. R.; Leone, S. R., *Phys. Rev. A* **2013**, *88*, 023420.

44. Dutoi, A. D.; Leone, S. R., *Chem. Phys.* **2017**, *482*, 249-264.

45. Neville, S. P.; Averbukh, V.; Ruberti, M.; Yun, R.; Patchkovskii, S.; Chergui, M.; Stolow, A.; Schuurman, M. S., *J.Chem. Phys.* **2016**, *145*, 144307.

46. Attar, A. R.; Bhattacherjee, A.; Leone, S. R., *J. Phys. Chem. Lett.* **2015**, *6*, 5072-5077.

47. Bhattacherjee, A.; Attar, A. R.; Leone, S. R., *J.Chem. Phys.* **2016**, *144*, 124311.

48. Zhang, Y.; Biggs, J. D.; Healion, D.; Govind, N.; Mukamel, S., *J.Chem. Phys.* **2012**, *137*, 194306.

49. Runge, A.; Gross, E. K. U., *Phys. Rev. Lett.* **1984**, *52*, 997-1000.

50. Gilbert, A. T. B.; Besley, N. A.; Gill, P. M. W., *J. Phys. Chem. A* **2008**, *112*, 13164–13171.

51. Hanson-Heine, M. W. D.; George, M. W.; Besley, N. A., *J.Chem. Phys.* **2013**, *138*, 064101.

52. Stener, M.; Fronzoni, G.; de Simone, M., *Chem. Phys. Lett.* **2003**, *373*, 115-123.

53. Lackner, F.; Chatterley, A. S.; Pemmaraju, C. D.; Closser, K. D.; Prendergast, D.; Neumark, D. M.; Leone, S. R.; Gessner, O., *J.Chem. Phys.* **2016**, *145*, 234313.

54. Baldea, I.; Schimmelpfennig, B.; Plaschke, M.; Rothe, J.; Schirmer, J.; Trofimov, A. B.; Fanghanel, T., *J. Electron Spectrosc. Relat. Phenom.* **2007**, *154*, 109-118.

55. Grazioli, C.; Baseggio, O.; Stener, M.; Fronzoni, G.; de Simone, M.; Coreno, M.; Guarnaccio, A.; Santagata, A.; D'Auria, M., *J.Chem. Phys.* **2017**, *146*, 054303.

56. Elsayed, M. A., *J.Chem. Phys.* **1963**, *38*, 2834-2838.

57. Soep, B.; Mestdagh, J. M.; Briant, M.; Gaveau, M. A.; Poisson, L., *Phys. Chem. Chem. Phys.* **2016**, *18*, 22914-22920.

58. Gerbich, T.; Schmitt, H.-C.; Fischer, I.; Mitric, R.; Petersen, J., *J. Phys. Chem. A* **2016**, *120*, 2089-2095.

59. Coe, J. D.; Martinez, T. J., *J. Am. Chem. Soc.* **2005**, *127*, 4560-4561.

60. Coe, J. D.; Martinez, T. J., *J. Phys. Chem. A* **2006**, *110*, 618-630.

61. Spighi, G.; Gaveau, M. A.; Mestdagh, J. M.; Poisson, L.; Soep, B., *Phys. Chem. Chem. Phys.* **2014**, *16*, 9610-9618.

62. Snellenburg, J. J.; Laptenok, S.; Seger, R.; Mullen, K. M.; Van Stokkum, I. H. M., *J. Stat. Softw*. **2012**, *49*, 1-22.

63. Lee, A. M. D.; Coe, J. D.; Ullrich, S.; Ho, M. L.; Lee, S. J.; Cheng, B. M.; Zgierski, M. Z.; Chen, I. C.; Martinez, T. J.; Stolow, A., *J. Phys. Chem. A* **2007**, *111*, 11948-11960.

64. McFarland, B. K.; Farrell, J. P.; Miyabe, S.; Tarantelli, F.; Aguilar, A.; Berrah, N.; Bostedt, C.; Bozek, J. D.; Bucksbaum, P. H.; Castagna, J. C.; Coffee, R. N.; Cryan, J. P.; Fang, L.; Feifel, R.; Gaffney, K. J.; Glownia, J. M.; Martinez, T. J.; Mucke, M.; Murphy, B.; Natan, A.; Osipov, T.; Petrovic, V. S.; Schorb, S.; Schultz, T.; Spector, L. S.; Swiggers, M.; Tenney, I.; Wang, S.; White, J. L.; White, W.; Gühr, M., *Nat. Commun.* **2014**, *5*, 4235.

65. Wolf, T. J. A.; Myhre, R. H.; Cryan, J. P.; Coriani, S.; Squibb, R. J.; Battistoni, A.; Berrah, N.; Bostedt, C.; Bucksbaum, P.; Coslovich, G.; Feifel, R.; Gaffney, K. J.; Grilj, J.; Martinez, T. J.; Miyabe, S.; Moeller, S. P.; Mucke, M.; Natan, A.; Obaid, R.; Osipov, T.; Plekan, O.; Wang, S.; Koch, H.; Gühr, M., *Nat. Commun.* **2017**, *8*, 29.

66. Livingstone, R.; Schalk, O.; Boguslavskiy, A. E.; Wu, G. R.; Bergendahl, L. T.; Stolow, A.; Paterson, M. J.; Townsend, D., *J.Chem. Phys.* **2011**, *135*, 194307.

67. Pemberton, C. C.; Zhang, Y.; Saita, K.; Kirrander, A.; Weber, P. M., *J. Phys. Chem. A* **2015**, *119*, 8832-8845.

TOC Graphic